# Dynamical Properties of the Thick Ascending Limb (TAL): A Modeling Study

Aniel Nieves-González[1], Chris Clausen[2], Harold E Layton[1], Anita T Layton[1], Leon C Moore[2]

[1]Mathematics, Duke University, Durham, NC; [2]Physiology, Stony Brook University, Stony Brook NY

## Program No. 665.8

We developed a cell-based model of the TAL with tubular inflow modulated by an empirical tubuloglomerular feedback (TGF) model to study the dynamical properties of the TAL. The cell-based TAL model tracks the time evolution and space dependency of cell volume and the luminal and cytosolic concentrations of major solutes including $Na^+$, $K^+$, $Cl^-$ and $NH_4^+$. The TAL segment model consists of a stack of cell models that comprise the wall. Each cell model includes detailed representations of the major transport pathways (NKCC2, KCC4, NHE3, BCE) as well as electrodiffusion. Cell volume and pH regulation are also included in the model. We simulated the TAL with and without the TGF system using different tubular fluid inflow forcing schemes and computed transfer, covariance, and coherence functions for the TAL cells to characterize the input-output relationships for each solute. The results, at the segmental level, verified our earlier findings (obtained with a much simpler TAL model) that the TAL acts as a nonlinear low-pass filter with a characteristic harmonic structure. In addition, the results predict that the individual TAL cells also act as multi-input/multi-output low-pass filters. Moreover, the cells behave as delay elements with different time constants for each solute. This research was supported by NIH grants DK-89006, DK-42091, and NSF grant DMS-0701412.

## Introduction

The TAL behaves like a nonlinear low-pass filter with a harmonic structure determined by the steady-state transit time, has been explained in previous modeling studies [6, 7]. Additionally, when the TGF loop is closed, the nonlinearities are accentuated and the TGF resonant frequency is clearly observed in the power spectrum. We have developed a detailed, cell-based model of the TAL segment which we used to examine the impact of the complex transport mechanisms in TAL cells on the dynamics of the TAL and TGF system. While previous studies used a simple single-barrier model of TAL cell transport, we can now define the TAL cell's input/output relationships.

## Mathematical Model

The TAL segment model (Fig. 1a) consists of an ensemble of 70 model TAL cells that make up the tubule walls. The model tracks luminal and cytosolic concentrations of 12 solutes and cell volume. The model equations are based on mass and $H_2O$ conservation, electroneutrality, luminal $H_2O$ impermeability and assumes a well-stirred cytosol. Solute fluxes have electrodiffusive (GHK equation) and carrier-mediated components, while $H_2O$ flow is by osmosis. Buffers are handled using the isohydric principle and the equilibrium assumption. Based on [4] we implement a CVR function that maps cell volume to NKCC2 and KCC4 transporter density (Fig. 1b). When the CVR function is ON there is a prescribed max. and min. NKCC activity, and when it is OFF the activity defaults to its max. unless otherwise specified. Table 1 summarizes the model parameters. The model equations were numerically solved in MATLAB®.

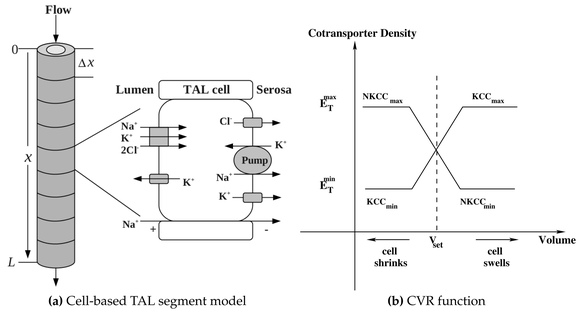


**(a)** Cell-based TAL segment model **(b)** CVR function

**Figure 1:** Model schematics.

**Table 1:** Model parameters[1]

| | apical[2] | basolateral[2] | value | reference |
|---|---|---|---|---|
| TAL radius | | | 10 $\mu$m | [5] |
| TAL length | | | 0.6 cm | [5] |
| baseline flow | | | 6 nL/min | [1] |
| TGF | | | | [6] |
| NKCC2A (OM,cTAL) | $\star$ | | | [9] |
| NKCC2B (cTAL) | $\star$ | | | [9] |
| KCC4 | | $\star$ | | [9] |
| NHE3 | $\star$ | $\star$ | | [11] |
| BCE | | $\star$ | | [2] |
| Na-K pump | | $\star$ | | [8, 12] |

[1] The parameter values were chosen to obtain tubular fluid dilution consistent with measurements by Vallon [10], and published data in isolated, perfused TAL segments [3].

[2] $\star$ means carrier is embedded in the cell membrane.

## Results

A series of simulations were done with the TAL model under different tubular inflow forcing schemes. Fig. 2 displays concentration profiles for with the TGF loop open during sinusoidal forcing with a frequency $1/t_{tt}$ Hz, where $t_{tt}$ is steady-state transit time. As observed in [6], the range of the excursions of $Cl^-$ concentration at the macula densa is larger when compared with a higher frequency forcing (see Fig. 3). This finding indicates that the TAL acts as a low pass filter. Likewise, the emergence of standing waves in $Na^+$ and $Cl^-$ profile are evident. The nodes of the standing waves are less definitive for $K^+$ and $NH_4^+$; this is a consequence of apical membrane cycling of these ions. Note that the cytosolic concentrations are not substantially perturbed by the oscillations in luminal concentrations because of cell volume regulation.

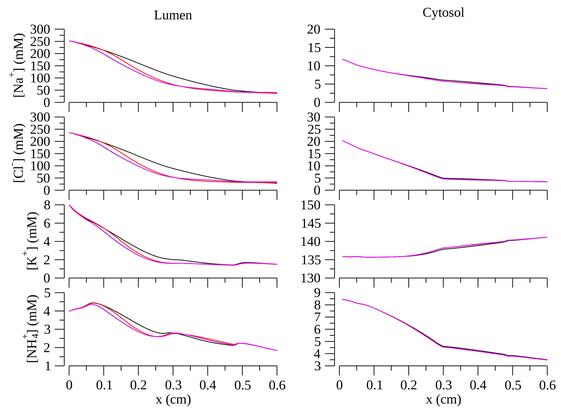


**Figure 2:** Luminal and cytosolic concentration profiles along the tubule when a $1/t_{tt}$ frequency sinusoidal forcing is applied. This is given at different times where the times are multiples of the sinusoidal period ($p$), so the colors of depicted curves which are black, red, green, blue, and magenta correspond to times $0p$, $p$, $2p$, $3p$ $4p$ respectively.

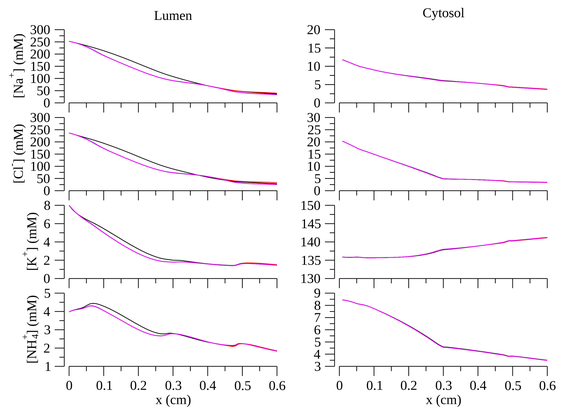


**Figure 3:** Luminal and cytosolic concentration profiles along the tubule when a $1.5/t_{tt}$ frequency sinusoidal forcing is applied. This is given at different times where the times are multiples of the sinusoidal period ($p$), so the colors of depicted curves which are black, red, green, blue, and magenta correspond to times $0p$, $p$, $2p$, $3p$ $4p$ respectively.

Figure 4 shows the time course at rwo locations in the TAL when a $2/t_{tt}$ frequency sinusoidal forcing is applied to the system with and without the TGF loop closed. Observe the distortion of the sinusoidal flow when the TGF loop is closed. Note that the cytosolic $[Cl^-]$ waveform is both atenuated and smoothed relative to the luminal waveform which suggests that the TAL cells act as low-pass filters.

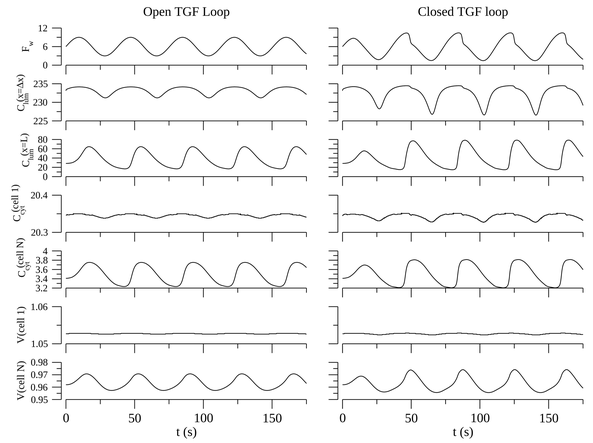


**Figure 4:** Time evolution for cytosolic and luminal $[Cl^-]$ (mM). Open TGF loop means a sinusoidal TAL inflow forcing. Closed TGF loop means that TGF inflow (nL/min) and sinusoidal forcing was applied. $V$ is normalized cell volume, and the IM-OM boundary is the start of the TAL.

Next, we applied a broad-band forcing, which consists of many oscillatory components over a band of the frequency spectrum. The frequencies of the forcing were prescribed up to the Nyquist frequency ($1/(2\Delta t) = 4642$ mHz) to avoid aliasing.

The power spectra obtained with a broad-band forcing and the TGF loop is closed is shown in Figure 5. Note that the PSD of the inflow (first panel) exhibits a peak at 35 mHz, the TGF resonance frequency, but the harmonic structure and filtering properties remains unchanged when compared to the open loop case (not shown). As noted previously in [6, 7], we observe in the $[Cl^-]$ PSD plots of Fig. 5 that the TAL behaves like a low-pass filter. Also, the location of the nodes in the PSD correspond to frequencies at which the local minima for magnitude in MD excursions were observed (not shown); these frequencies are those where the oscillatory flow transit time is a multiple of the steady-state transit time [7].

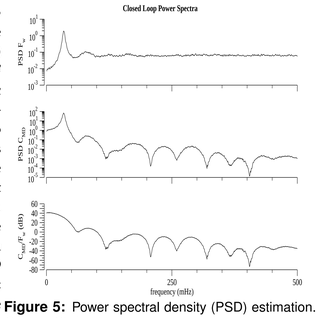


**Figure 5:** Power spectral density (PSD) estimation. $C_{MD}$ is $[Cl^-]$ at the macula densa.

Fig. 6 shows the ratio of PSD functions of cytosolic to luminal concentrations. If the cells are assumed to be ideal multi-input/multi-output systems, then each panel can be interpreted as a plot of the gain factor of the system (cell) as a function of frequency. We observe that for $K^+$ and $Cl^-$ the gain tends to increase from OM to cortex. $Na^+$ and $Cl^-$ have negative gain values, which indicates input-to-output (I/O) attenuation. This explains the relatively small changes in cytosolic concentrations observed in the sinusoidal forcing simulations (see Figure 2). For $K^+$ in the cortical region the I/O relation is positive, which implies amplification.

In the cortico-medullary junction and late cortex the $Na^+$ and $Cl^-$ pair have a similar nodal structure (optima location). This grouping is due to the shared transport pathways that take the solutes across the apical membrane. Note that the optima locations in the PSDs of $Na^+$ and $Cl^-$ have simmilar nodal structure as in Fig. 5. Also, for $K^+$ and $NH_4^+$ in the late cortex, the waveforms of their I/O relationships seems to mirror one another. This reflects that these two solutes share transport pathways (NKCC2 and ion channels). Regardless of the solute and location, the TAL cells behave like low-pass filters. Hence because, in practice, a delay element turns into a low-pass filter with a phase shift, we claim that TAL cells behave like delay elements with different time constants for each solute. Fig. 7 shows the I/O correlation for $Na^+$. The non-zero location for the maximum indicates that the output is indeed being delayed w/respect to the input.

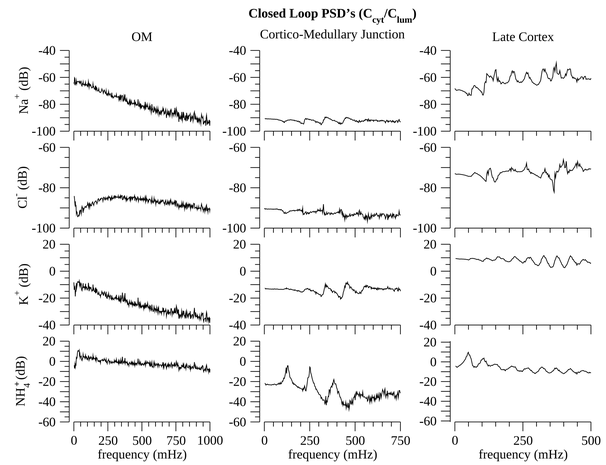


**Figure 6:** Input-output relation (frequency response). OM is outer medulla.




**Figure 7:** Cross-Correlation: $C_{lum}$ to $C_{cyt}$.

## Conclusions

The major results of this modeling study are:

- When TAL inflow oscillates the TAL segment acts as a nonlinear low-pass filter with a characteristic harmonic structure. Such structure is derived from tubule properties like the steady-state transit time, and reflects the establishment of standing waves of $Na^+$ and $Cl^-$ in the lumen of the TAL. This finding is consistent with both earlier modeling efforts and experimental data.
- The harmonic structure is affected by the transport properties of the solute under consideration.
- The TAL cells themselves are predicted to act as multi-input/multi-output nonlinear filters.

## References

[1] C. de Rouffignac et al. *Pflugers Archive*, 317:141–156, 1970.
[2] H. C. et al. *Am. J. Physiol. Renal*, 281:F222–F243, 2001.
[3] R. Greger. *Physiol. Rev.*, 65:760–797, 1985.
[4] K. Kahle et al. *P NAS*, 101:2064–2069, 2004.
[5] M. Knepper ar al. *Kidney International*, 12:313–323, 1977.
[6] H. Layton et al. *Am. J. Physiol. Renal Physiol*, 273:F625–634, 1997.
[7] H. Layton et al. *Am. J. Physiol. Renal Physiol*, 273:F635–F649, 1997.
[8] C. Luo et al. *Circ Res*, 74:1071–1096, 1994.
[9] M. Marcano et al. `http://ccom.uprrp.edu/~mmarcano/manuscripts/NKCC2_KCC_NH4.pdf`.
[10] V. Vallon et al. *JASN*, 8:1831–37, 1997.
[11] A. Weinstein. *J. Gen. Physiol.*, 105:617–641, 1995.
[12] A. Weinstein et al. *Am. J. Physiol. Renal Physiol.*, 298:F525–F542, 2010.